Machine learning application to space particle discrimination from multiple-cell upsets in a memory device

Andrea Coronetti, Lucas Matana Luza, Sanaa Barik, Alexandre Bosser, Ruben Garcia Alia, Luigi Dilillo, Frédéric Saigné

Title: Machine learning application to space particle discrimination from multiple-cell upsets in a memory device

Author(s): Andrea Coronetti, Lucas Matana Luza, Sanaa Barik, Alexandre Bosser, Rubén García-Alía, Luigi Dilillo, and Frédéric Saigné

Document version: Post-print version (Final draft)

Please cite the original version:
A. Coronetti *et al.*, "Machine learning application to space particle discrimination from multiple-cell upsets in a memory device," 2022 European Conference on Radiation and Its Effects on Components and Systems (RADECS), 2022, pp. 1-4.

Machine learning application to space particle discrimination from multiple-cell upsets in a memory device

Andrea Coronetti, Lucas Matana Luza, Sanaa Barik, Alexandre Bosser, Rubén García-Alía, Luigi Dilillo, and Frédéric Saigné.

Abstract

Machine learning algorithms are set-up to enable particle detection in the mixed-field space environment starting from the MCUs collected in an SRAM during ground irradiations with protons and ions.

Index Terms

Machine learning, particle detection, LET detection, Multiple-Cell-Upsets, memory, space environment.

I. Introduction

MULTIPLE-cell upsets (MCUs) have become the dominant contributor to the single-event upset (SEU) count rate for memory devices based on nanometric technologies. Furthermore, these memory devices are not only susceptible to SEUs from heavy ions and high-energy protons, but also from low-energy proton through direct ionization.

MCUs occur whenever the energy deposited by a single-particle is not collected solely at the cell where the particle stroke, but is diffused and collected at the sensitive nodes of other physically adjacent or electrically connected cells, resulting in a larger amount of bit-flips.

MCUs can impact the reliability of data stored in memories and memory-based devices in electronic systems exposed to radiation. However, bit interleaving (bits belonging to the same word not placed in physically adjacent cells) improves the effectiveness of error detection and correction instrumentation and can help alleviating the related issues.

When it comes to commercial electronics, the details behind the scrambling algorithms and the bit interleaving schemes, which are useful to define the physical bitmaps, are typically not available. The absence of the logical-to-physical mask may thus prevent determining whether the observed SEUs during a test are single-bit upsets (SBUs) or MCUs.

When this information is available, sometimes complemented with cell topology and transistor/circuits layout, it can be used to model the physical and electrical processes at the origin of MCUs [1–4].

MCUs may also affect the execution of machine learning (ML) algorithms embedded in high-performance memory-based devices that can be used to implement tasks such as image processing and complex autonomous decision-making directly on-board satellites. Indeed, the use of machine learning and deep learning techniques and their reliability under radiation is a current topic of investigation within the radiation effect community [5–7].

Other than for its performance under radiation, machine learning is finding application in radiation effect data analysis and on-board anomaly detection and predictions [8–10].

In this work, ground facility measurements of MCUs in a 65 nm commercial static random access memory (SRAM) are analysed, classified and submitted to machine learning algorithms with the aim of using it as a potentially cheap particle detector in space for flux measurements or solar particle events. [For the final paper we will also include the

This study has received funding from the European Union's Horizon 2020 research and innovation programme under the MSC grant agreement no. 721624.

Andrea Coronetti (andrea.coronetti@cern.ch) is with CERN, CH-1211 Geneva, Switzerland and with Institute d'Électronique et des Systèmes, Université de Montpellier, 34090 Montpellier, France.

Lucas Matana-Luza and Luigi Dilillo are with LIRMM, Univ Montpellier, CNRS, 34095 Montpellier, France.

Sanaa Barik is with CERN, CH-1211 Geneva, Switzerland and with LIRMM, Univ Montpellier, CNRS, 34095 Montpellier, France.

Alexandre Bosser is with LIRMM, Univ Montpellier, CNRS, 34095 Montpellier, France, and with 3DPlus, 78530 Buc, France.

Rubén García Alía is with CERN, CH-1211 Geneva, Switzerland.

Frédéric Saigné is with Institute d'Électronique et des Systèmes, Université de Montpellier, 34090 Montpellier, France.

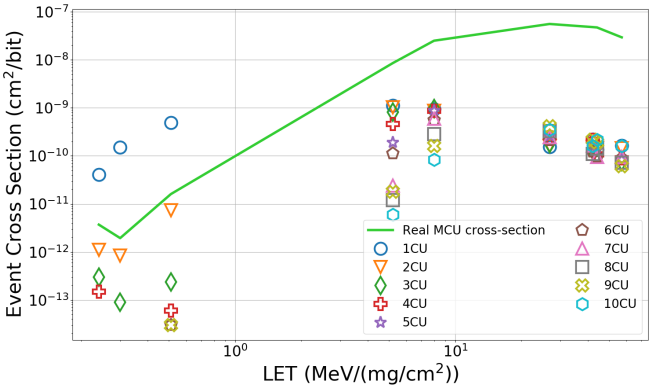

Fig. 1. MCU event cross-sections as a function of multiplicity (1-10) and total MCU cross-section (2-100) as a function of ion LET.

discrimination for the particle LET]. Two different approaches are investigated; the first is based on a parametrization of the MCU features that is then used by ML algorithms for fitting purposes; the second is based on running a convolutional neural network (CNN) directly on the MCU shapes to perform the particle discrimination. Such kind of implementations may then be used on-board spacecraft carrying a memory device to perform measurements of the space environment features.

II. Experimental Measurements at Ground Facilities

The targeted SRAM for this study is the CY62167GE30-45ZXI, commercially available from Infineon. The SRAM is based on a 65 nm technology, it has a capacity of 16 Mbits. During the tests it was biased at 3.3 V and written with a logical checkerboard pattern. To be noted that the commercial version embeds an error correction code that was disabled for the purpose of these tests in order to get a larger sample of upsets. The logical-to-physical mapping is also available from the LIRMM-Infineon collaboration.

The raw SEU cross-sections for these experiments were published in [11]. However, no details about the MCUs were extracted at the time of publishing that paper due to the lack of the logical-to-physical mapping. The data presented in this paper are limited to ion and proton measurements performed at UMCG-PARTREC [12], GANIL [13] and CNA [14].

It shall be mentioned that, differently from the ions in the space environment, the ions used at ground facilities were C, Ar and Xe with energies limited to 30-90 MeV/n and at normal incidence. Therefore the MCUs from galactic cosmic rays (GCRs) may not match those obtained in low-energy facilities due to the different ionization track structures [15]. [We plan to collect additional data at GSI with high-energy Fe and U ($>$ 100 MeV/n) at similar linear energy transfer (LET) to have a more complete picture.]

Ion irradiations were performed in air on delidded samples. Low-energy proton ($<$20 MeV) irradiations were performed in vacuum on delidded samples. High-energy proton irradiations ($>$20 MeV) were performed in air on packaged samples. The MCUs were extracted from the raw data and classified following the methodology presented by LIRMM [16, 17].

All the observed MCUs have a multiplicity $m < 50$. For each value of m it is possible to calculate a mCU event cross-section. These cross-sections are shown, as a function of LET, for ions in Fig. 1, and, as a function of energy, for protons, in Fig. 2, for m = 1-10. In addition, the figures also report the total MCU cross-section, which is defined as the sum of all cross-section with $m > 2$:

$$\sigma_{MCU,total} = \sum_{m=2}^{100} m \cdot \sigma_{mCU,event} \tag{1}$$

As shown in the figures, MCUs are very rare in the case of low-energy protons and low-LET ions, i.e., they are typically just 1% of the total SEUs. Given that the MCU total cross-section reaches the same value as the 1CU cross-section for protons with energy $>$ 20 MeV, 50% of the total bit in errors from high-energy protons belong to MCUs. For intermediate and high LET ions, the MCU total cross-section can grow to become 100-1000 times higher than the 1CU cross-section, meaning that 99-99.9% of the total bit in errors belong to MCUs.

It may also be worthwhile plotting a histogram of the MCU multiplicity distribution for intermediate and high-LET ions, as done in Fig. 3. It is evident that the maximum multiplicity increases as the LET increases. However, it is

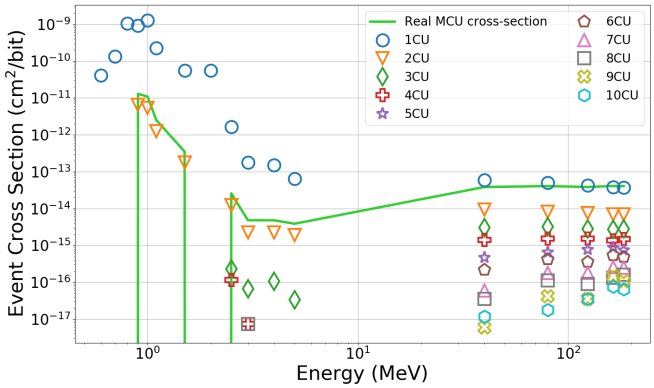

Fig. 2. MCU event cross-sections as a function of multiplicity (1-10) and total MCU cross-section (2-100) as a function of proton energy.

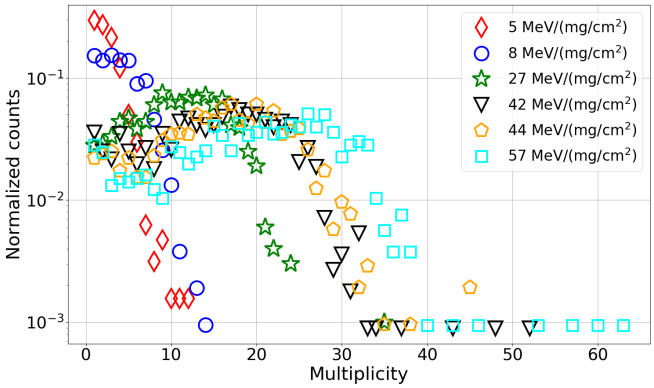

Fig. 3. Histogram of MCU multiplicity distribution as a function of the ion LET.

noteworthy that the multiplicity distributions of each high-LET ion from 1 to 25 are almost flat. This means that there seem to be equal probability for an ion passing through the device to cause events with m in the 1-25 interval.

III. Analysis and Parametrization of MCU Clusters

In order to predict whether a certain MCU is caused by a proton or an ion some features of the MCU clusters can be classified. Fig. 4(a) is the map of an MCU cluster with high multiplicity caused by a high-LET ion. The bits in error are sparsely distributed and sometimes not physically adjacent. Since this is a common situation, the following parameters are considered in order to classify the various MCU clusters:

- the multiplicity, m;
- the horizontal width (bit-line), Δx;
- the vertical width (word-line), Δy;
- the fill-factor of the cluster, $f = \frac{m}{\Delta x \Delta y}$

For instance, in the example in the figure, the cluster will be classified as having m = 24, Δx = 5, Δy = 10 and f = 0.48. With these parameters, the MCU clusters of each particle (and LET/energy) can be classified by means of 2D heatmaps showing the probability that an ion/proton will produce clusters with a certain combination of Δx-Δy.

Plots for such heatmaps are reported in Fig. 4(b-f) for low-energy protons (b), high-energy protons (c), low-LET ions (d), intermediate-LET ions (e) and high-LET ions (f). The heatmaps thus provide an idea of the most likely horizontal and vertical sizes of the MCU clusters. For instance, looking at the three ion plots it can be seen that the maximum likelihood moves towards higher horizontal and vertical width as the ion LET is increased.

From the heatmaps it is also noted that for low-energy protons and low-LET ions, the MCU clusters tend to have a similar size along the two directions. On the other hand, as the LET increases (secondary ions from high-energy protons have low- and intermediate-LETs) the shape of the MCUs tends to be stretched along the vertical direction, often with a 2:1 ratio with respect to the horizontal direction.

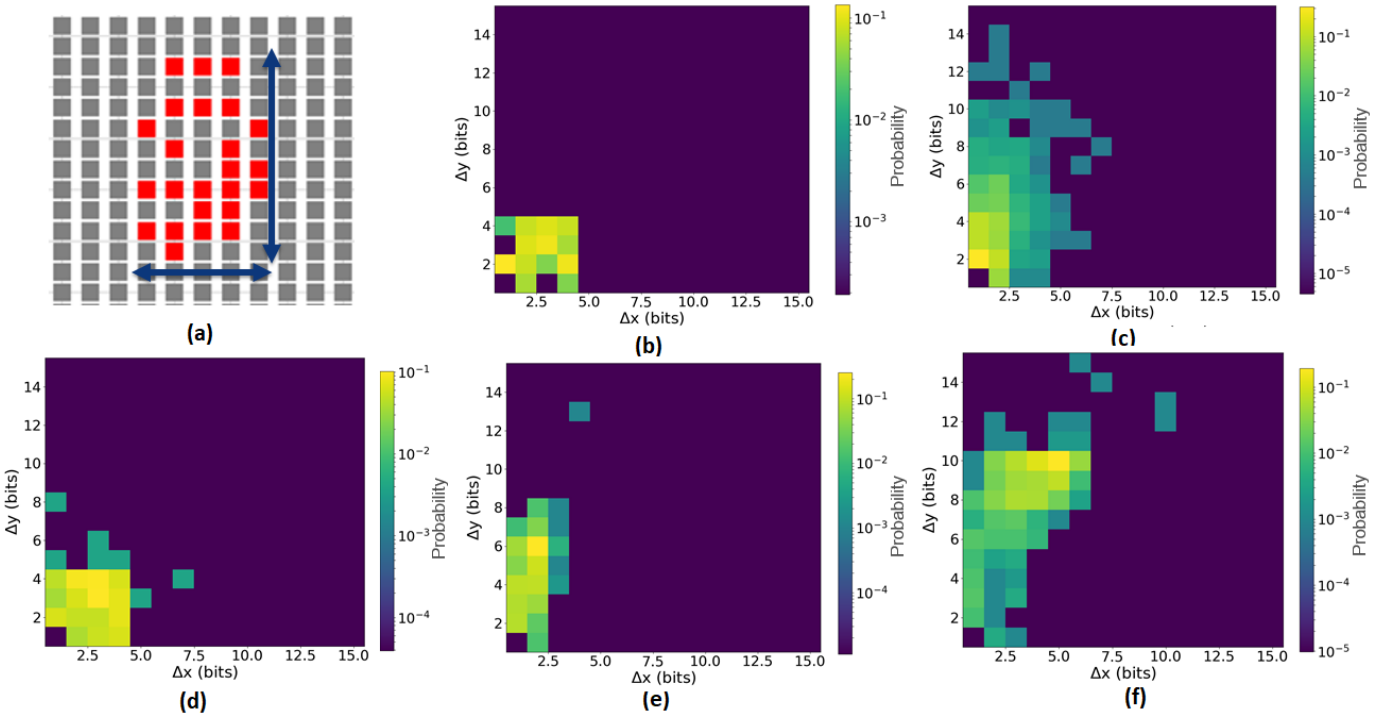

Fig. 4. (a) 2D example of an ion cluster with m = 24 (bits in error are marked in red); guidelines in blue are drawn on top to show quantities used for the parametrization of the clusters. (b-f) heatmaps of MCU clusters based on the combinations of Δx-Δy. Beams: (b) 0.9 MeV protons, (c) 190 MeV protons, (d) 360 MeV C (0.51 MeV/(mg/cm^2)), (e) 550 MeV Ar (8.2 MeV/(mg/cm^2)), (f) 2700 MeV Xe (43.5 MeV/(mg/cm^2)).

It is also noteworthy that for high-energy protons, whereas very large MCU clusters are possible, typically the most likely are still those that have a 2:1 shape. [Concerning the fill-factor and its added value, these will be presented in more detail in the final paper].

As it can be seen comparing plots (b) and (d), the proposed parameters do not seem as effective when it comes to differentiate low-energy protons and low-LET ions (both SEU mechanisms caused by direct ionization) that share a very similar LET.

IV. Machine Learning Applied to Particle Discrimination

For the parametric fitting, a dataset of MCUs measured at the facility (comprising $>$ 18000 MCU clusters) is built, including information about the particle type, energy, LET, m, Δx, Δy and f. On the other hand, for the CNN image recognition algorithm, images such as Fig. 4(a) are directly submitted to the model training process with just a label to mark the difference between ion and proton MCUs.

For the parametric fitting, a normalization is done to rescale the analogue values of the parameters m, Δx, Δy and f, so that they can only have value between $\pm$1. This will facilitate the task of the ML algorithm in fitting the data.

Both ML algorithms are meant at performing a simple binary classification to discriminate whether the particles in the testing dataset are ions or protons. The algorithms are trained with 50% of the MCU cluster dataset (including low- and high-energy protons and ions of any LET) and tested against the remaining 50%.

For the parameter fitting, some ML classification algorithms, available through python scikit-learn, were implemented and, more or less, all of them returned very similar results. Typically, the classification algorithm is capable of correctly identifying 88% of the particles that are at the origin of a certain MCU. The remaining 12%, as indicated in Fig. 5, are low- and intermediate-LET ions that are mistaken for protons. Concerning the other particles, typically the accuracy for high-energy proton MCUs is $>$ 95%, whereas for high-LET ions the identification is successful in $>$ 80% of the cases and growing with increasing LET.

Concerning the CNN for image recognition, this is developed with tensorflow keras python libraries. In this case the algorithm is not prompted with any parameter, but it is left performing the data analysis and devise the model based on the MCU shapes. In spite of the very different approach, the algorithm returns again an accuracy of 88%.

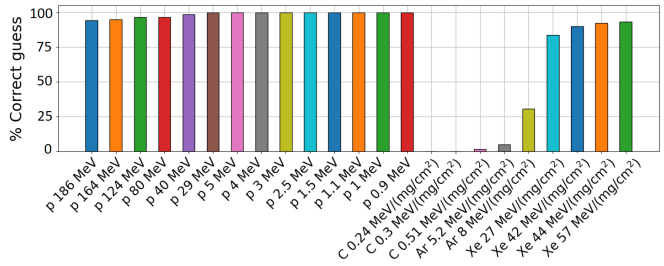

Fig. 5. Binary classification accuracy of the parametric fitting ML model for each ion and proton run.

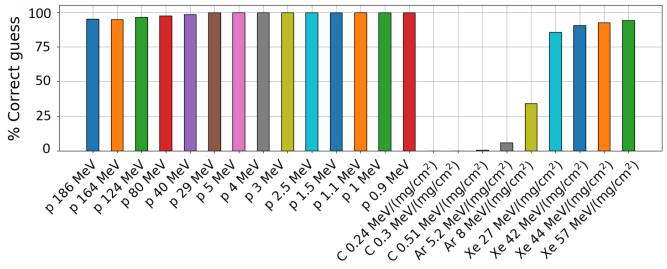

Fig. 6. Binary classification accuracy of the CNN image recognition model for each ion and proton run.

As can be seen in the detailed histogram in Fig. 6, similar conclusions to the parameter fitting apply and the image recognition algorithm converged to a model that considers low-LET ions to be low-energy protons.

The fact that ML algorithms running with less than a handful of parameters to perform the fit provide very similar accuracy to an image recognition CNN confirms the good parametrization enforced on the MCU clusters. In addition, the parametric fit algorithms are much faster than the image recognition CNN. [In the final paper, the analysis will be further revised and refined and more statistics on algorithm evaluation will be provided].

The fact that low-energy protons and low-LET ions yield similar MCU shapes is not surprising considering that both energy deposition mechanisms are direct ionization driven and that the particles share pretty similar LETs. The only big difference would be related to the different ionization tracks, that are much longer for 90 MeV/n ions than 1-3 MeV protons, but this does not seem to produce significant effects on the MCU characteristics.

V. Conclusions

The paper reports a data analysis of MCUs measured at proton and ion facilities for a 65 nm bulk SRAM. The data shows that 50% of the upsets from high-energy protons and 99% of the upsets from high-LET ions belong to MCUs. Given this overwhelming majority, MCUs are further analysed and parametrized to provide better discrimination tools between the particles behind the feature of a certain MCU. It is shown that while for low-LET particles the shape of MCUs is typically symmetric in the bit- (x) and word-line (y) directions, as the LET (or the energy for protons) grows the MCU tend to stretch and tend to spread over several word-lines.

Both the raw MCU image and the parametrized MCU data can be used as input to ML algorithms. Both the image recognition CNN and the parametric fitting demonstrated equal accuracy and the ability to discriminate high-energy proton and high-LET ion MCUs (which are the most likely in the space environment considering the cross-sections). However, they could not succeed in discriminating MCUs caused by low-LET particles (for what matters a pure binary classification as either protons or ions). The overall capabilities of using these schemes for particle detection in space will be assessed in the final paper.

References

[1] Y.-P. Fang and A.S. Oates, “Characterization of single bit and multiple cell soft error events in planar and FinFET SRAMs,” *IEEE Trans. Dev. Mat. Rel.*, vol. 16, no. 2, pp. 132-137, June 2016.

[2] T. Kato et al., “The impact of multiple-cell charge generation on multiple-cell upset in a 20-nm bulk SRAM,” *IEEE Trans. Nucl. Sci.*, vol. 65, no. 8, pp. 1900-1907, Aug. 2018.

[3] G. Gasiot, D. Giot, and P. Roche, “Multiple cell upsets as the key contribution to the total SER of 65 nm CMOS SRAMs and its dependence on well engineering,” *IEEE Trans. Nucl. Sci.*, vol. 54, no. 6, pp. 2468-2473, Dec. 2007.

[4] D. Giot, P. Roche, G. Gasiot, J.-L. Autran, and R. Harboe-Sorensen, “Heavy ion testing and 3D simulations of multiple cell upset in 65nm standard SRAMs,” *Proc. RADECS Conf.*, Deauville, France, 2007.

[5] M.G. Trinidade et al., “Assessment of a hardware-implemented machine learning technique under neutron irradiation”, *IEEE Trans. Nucl. Sci.*, vol. 66, no. 7, pp. 1441-1448, July 2019.
[6] R.B. Jacobs-Gedrim et al., “Training a neural network on analog TaOx ReRAM devices irradiated with heavy ions: effects on classification accuracy demonstrated with CrossSim,” *IEEE Trans. Nucl. Sci.*, vol. 66, no. 1, pp. 54-60, Jan. 2019.
[7] L. Matana Luza et al., “Emulating the effects of radiation-induced soft-errors for the reliability assessment of neural networks,” *IEEE Trans. Emerg. Topics Comput.*, available online: https://doi.org/10.1109/TETC.2021.3116999.
[8] T.D. Loveless, D.R. Reising, J.C. Cancelleri, L.W. Massengill, and D. McMorrow, “Analysis of single event transients (SET) using machine learning (ML) and ionizing radiation effects spectroscopy (IRES),” *IEEE Trans. Nucl. Sci.*, vol. 68, no. 8, pp. 1600-1606, Aug. 2021.
[9] A. Ildefonso et al., “Using machine learning to mitigate single-event upsets in RF circuits and systems,” *IEEE Trans. Nucl. Sci.*, vol., no., pp., month 2022.
[10] D.L. Hansen, D. Czajkowski, and B. Vermeire, “Using machine learning to determine proton cross-sections from heavy-ion data,” *IEEE Trans. Nucl. Sci.*, vol., no., pp., month 2022.
[11] A. Coronetti et al., “SEU characterization of commercial and custom-designed SRAMs based on 90-nm technology and below,” *in IEEE Radiation Effects Data Workshop Rec.*, Santa Fe, NM, USA, Dec. 2020, pp. 56-63.
[12] E.R. van der Graaf, R.W. Ostendorf, M.J. van Goethem, H.H. Kiewiet, M.A. Hofstee, and S. Brandenburg, “AGORFIRM, the AGOR facility for irradiations of material,” *in Proc. 2009 RADECS Conf.*, Bruges, Belgium, Sept. 2009, pp. 451-454.
[13] M.-H. Moscatello, A. Dubois, and X. Ledoux, “Industrial applications with GANIL SPIRAL2 facility,” *Proc. RADECS Conf.*, Bremen, Germany, 2016.
[14] Y. Morilla et al., “Progress of CNA to become the spanish facility for combined irradiation testing in aerospace,” *in Proc. 2018 RADECS Conf.*, Gothenburg, Sweden, Sept. 2018, pp. 250-254.
[15] M.P. King et al., “The impact of delta-rays on single-event upsets in highly scaled SOI SRAMs,” *IEEE Trans. Nucl. Sci.*, vol. 57, no. 6, pp. 3169-3175, Dec. 2010.
[16] G. Tsiligiannis et al., “Multiple cell upset classification in commercial SRAMs,” *IEEE Trans. Nucl. Sci.*, vol. 61, no. 4, pp. 1747-1754, Aug. 2014.
[17] A. Bosser et al., “Investigation on MCU clustering methodologies for cross-section estimation of RAMs,” *IEEE Trans. Nucl. Sci.*, vol. 62, no. 6, pp. 2620-2626, Dec. 2015.